3-Pass D-InSAR for Estimation of Displacements Caused by October 2016 Central Italy Earthquake

Cosmin Dănișor, University Politehnica of Bucharest, cosmin.danisor@yahoo.com, Romania
Mihai Datcu, German Aerospace Center, Mihai.datcu@dlr.de, Germany

Abstract

The choice between 2-pass or higher order pass D-InSAR algorithms to separate the displacements component of the interferometric phase represents a trade-off between the necessity to re-sample and coregister a low resolution external DEM to SAR acquisition geometry, and the necessity to unwrap an interferometric phase which contains the topographic component. Majority of works carried in this domain prefer the use of 2-pass D-InSAR algorithm. In this paper, reliable results are obtained by implementation of a 3-pass differential interferometric processing chain to estimate the displacements caused in Perugia region, Italy, by the earthquake which occured on 30.10.2016.

1 Introduction

Synthetic Aperture Radars (SAR) [1] are active illuminating systems operating in microwaves domain that exploit the Doppler history of signals operated by sensors mounted on a platform which moves with a constant velocity relative to the illuminated scene. Usually, the platform is an aircraft (in case of airborne SAR systems) or a satellite (spaceborne systems). Main advantages compared to optical sensors consist in the capability to acquire the data independently of weather conditions and sunlight. SAR are coherent systems, which use quadrature modulation [1] to exploit both amplitude and phase of backscattered echoes. Because of the relative movement between sensor and scene, a large antenna is synthesized, thus offering the possibility of improving the azimuth resolution without extending the physical dimensions of the antenna. The width of the transmitted pulses represents a compromise between the achievable signal to noise ratio and the range resolution. To achieve an equitable trade-off between those two parameters most systems use phase coded waveforms [2]: the chirp signals.

SAR interferometry [3] analyses the phase difference between at least two focused images. If two acquisitions are made from different sensor positions in a short temporal interval, topographic component can be separated from the interferometric phase and processed to generate accurate digital elevation models (DEM) of the scene.

Differential interferometry (D-InSAR) [4] aims to estimate the scene's displacements by separating the corresponding deformation component from the interferometric phase. To achieve this task, topographic component must be computed and subtracted from the interferograms. Initial approaches of this technique [5], employed between two and four complex acquisitions for displacements estimation. Two pass differential interferometry uses an external DEM to subtract the topographic component from the interferometric phase obtained by the two acquisitions. Three pass differential interferometry uses a pair of complex acquisitions for topographic phase estimation and another pair for computation of deformation component, the two pairs having a common master image. Four pass D-InSAR follows the same approach, but the two image pairs are independent.

This paper follows the subsequent structure: section 2 states the objectives, the employed dataset and justifies the preference for 3-pass D-InSAR. Section 3 presents the dataset's pre-processing step and section 4 describes the differential processing chain for displacements estimation. Results and conclusions are contained in sections 5 and 6.

2 Objectives

Main objective of this work consists in implementation of a processing chain for the estimation of the displacements generated by the major earthquake occurred on 30.10.2016 in central part of Italy, with epicentre in Perugia region. The advantage of availability of SAR data acquired by Sentinel-1 constellation in TOPS mode, which has large land coverage and short re-visit time will be exploited. Optical view and amplitude of SAR image which will be used as reference, from the epicentre region are presented in **Figures 1 and 2**:

ISBN 978-3-8007-4636-1 / ISSN 2197-4403

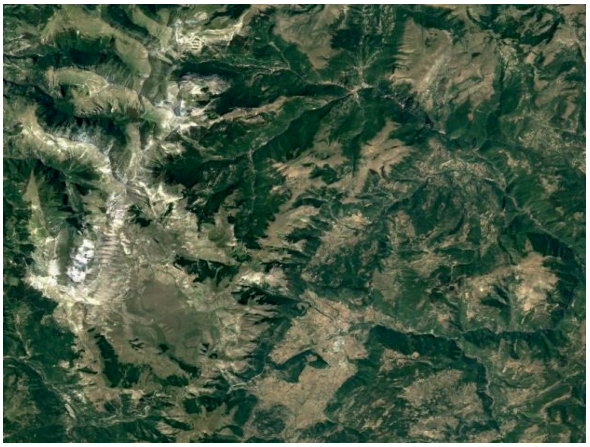

Figure 1: Optical view of epicentre region, Perugia

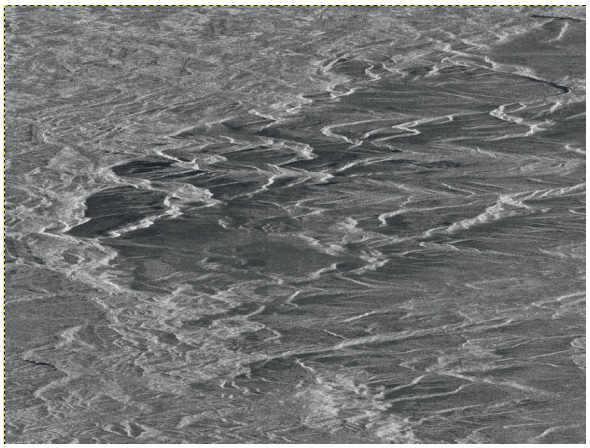

Figure 2: Amplitude of test region in Sentinel-1 image acquired on 14.10.2016

Interferometric phase Φ_{itf} [4] contains the contributions of scene's topography Φ_{topo}, earth's curvature Φ_{fl}, displacements Φ_{disp} and the residual component, which includes atmospheric phase screen effects Φ_{atm} and noise Φ_n:

$$\Phi_{itf} = \Phi_{topo} + \Phi_{fl} + \Phi_{disp} + \Phi_{atm} + \Phi_n \quad (1)$$

The displacements component Φ_{disp} is proportional to the terrain deformations δr which occurred between the acquisition moments of the interferometric images pair (λ is radar's wavelength):

$$\Phi_{disp} = \frac{4\pi}{\lambda}\delta r \quad (2)$$

An important challenge of differential interferometry consists in estimation and subtraction of topographic component, which is proportional to scene's height. Most papers which address the process of displacements estimation [6]-[7] adopt the use of an external DEM for displacements estimation to avoid the necessity of topographic phase unwrapping. In this article, the use of 3-pass D-InSAR is employed. This choice was preferred considering that the spatial resolution of most popular external DEM – SRTM, 90 or 30 m, is considerably lower than the one of Sentinel 1 images, 5 m in range and 20 m in azimuth for TOPS acquisition mode. Also, the DEM conversion from ground to SAR system's geometry and co-registration with dataset's images are avoided. The trade-off is given by the eventual difficulties that may occur during the phase unwrapping of an interferogram without subtracting the topographic phase first. Therefore, performant phase filtering and unwrapping algorithms need to be carefully implemented. 3 pass differential method was preferred instead the 4 pass one, because the common master image use avoids a supplementary co-registration step of topographic and differential image pair interferograms.

From the 3 acquisitions dataset, two images will form the topographic pair, which will be used for scene's topography estimation, and two images will form the differential pair, which represents the basics for displacements interferometric component separation. As mentioned, those two acquisition pairs have common master image. Both images of the topographic pair need to be acquired before natural disaster's occurrence. This pair requires short temporal baseline, to limit the effects of temporal decorrelation, and large perpendicular baseline, to maximize the sensitivity of interferometric phase's topographic component to terrain's altitude. Differential pair needs to have the master image acquired before and the slave image acquired after the earthquake's appearance. Ideally, the perpendicular baseline of the latter pair needs to be short, in order to maximize the interferometric phase's sensitivity to deformation effects. The structure of the 3 acquisitions dataset is presented in **Figure 3**:

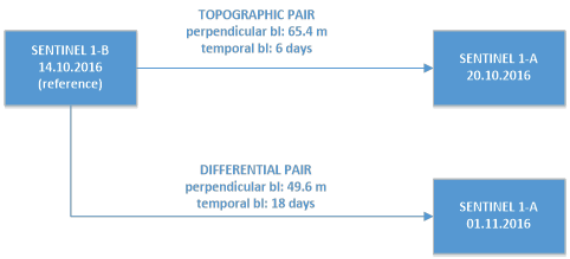

Figure 3: Dataset's acquisition dates and baselines

As it can be noticed, the perpendicular baseline of the topographic set is larger than the one of differential pair 65.46 m compared to 49.65 m. The temporal baseline of the topographic images has the smallest possible temporal baseline value – 6 days, this being possible after the launch of the second satellite of the Sentinel-1 constellation. The slave image of the differential pair is acquired two days after the earthquake's occurrence. The processing chain will be implemented by exploiting the functionalities of Gamma software's interferometric and differential interferometric packages [8]-[9].

ISBN 978-3-8007-4636-1 / ISSN 2197-4403

3 Dataset's pre-processing

To compensate the different acquisition geometries of dataset's images, slave images need to be resampled into master acquisition's geometry. In the case of Sentinel-1 images acquired in TOPS mode, co-registration process requires sub-pixel accuracy in azimuth direction, because of the presence of Doppler frequency shifts between consecutive bursts of the images. If this constraint is not met, those frequency shifts will be visible during the next processing steps, affecting the interferometric processing of the image pair.

This process is implemented in three steps [8]: coarse co-registration and two refinement iterations. Initial step estimates a set of constant offsets in both range and azimuth based on the orbital information of the acquisitions. Orbit state vectors of Sentinel-1 images are precise, so this step is expected to return reliable results. First refinement step computes the cross correlation of images intensities, in multiple patches defined across the scene. Variable offsets are determined based on cross-correlation maximization. Second refinement step is essential for avoiding the presence of Doppler frequency shifts in the interferograms generated from the co-registered pairs. Double phase difference is computed and minimized in bursts' overlap regions. Because those regions are essential for accuracy of resampling process in azimuth direction, co-registration step was implemented on whole images, after conduction of the de-bursting process. All overlap areas are analyzed to determine the best global offset in azimuth direction.

Validation of pre-processing step can be implemented by generating the interferogram of the co-registered pair. If no Doppler frequency shifts are visible, high precision alignment of dataset's images was achieved, both slave images being accurately resampled to master acquisition's geometry. For further processing, the test region presented in **Figure 2** will be separated from the co-registered dataset. This region contains 5000x5000 pixels, covering a surface of 808.52 km^2.

4 Differential processing chain

The same interferometric processing chain, whose steps are presented in **Figure 4**, is applied for both topographic and differential images pair. The two obtained unwrapped phases are then properly combined to estimate the displacements component

For interferogram computation, common band filtering is employed only in range direction, because of Doppler frequency shifts present in azimuth. Interferogram flattening is performed at this step in order to facilitate the unwrapping process. Earth's curvature phase trend is estimated based on orbital information. Interferometric phase filtering is an essential precursor of the unwrapping process. Phase noise is reduced without affecting interferogram's spatial resolution. An adaptive filtering process is implemented, the filter being adapted to interferogram's power spectral density [10].

$$H = |S|^{\alpha} \tag{3}$$

where H is the filter's transfer function, S represents the interferometric power spectral density, and α is a subunit coefficient which represents the attenuation of power spectral density's peak value. To achieve a compromise between SNR increase and loss of information alfa was set at 0.5

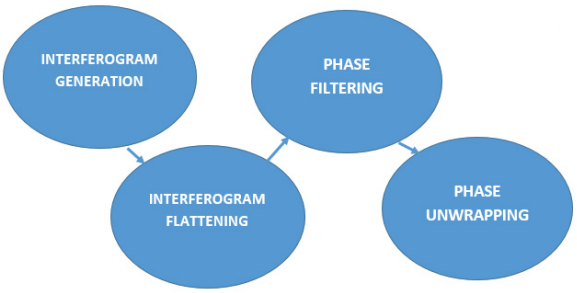

Figure 4: Main steps of interferometric and differential image pairs processing chain

During phase filtering, spectral coherence of the images is also estimated. This will represent an input argument for the unwrapping process. Special consideration is given to the unwrapping implementation, since it's the most critical part of the processing chain.

Phase unwrapping is conducted using the minimum cost flow algorithm (MCF) [11]. In first instance, areas characterized by low spectral coherence are masked, the unwrapping being carried in the selected seed points characterized by high coherence. Then, the solution is propagated by computation of Delaunay triangulation [12] in the range-azimuth plane.

The two unwrapped interferograms will be combined to estimate the displacements interferometric component. It is expected that topographic component is dominant in the first unwrapped phase. Therefore, this interferogram must be scaled to compensate the different perpendicular baselines of the image pairs, and then be subtracted from the interferogram of the differential pair. Before scaling and subtraction, earth's curvature phase trend, which was subtracted to facilitate the unwrapping process, must now be re-added to both interferograms. This is also required because of the different baselines of the image pairs.

The displacements information is expected to be dominant in the interferometric phase obtained after the combination of un-flattened interferograms, therefore the displacements caused by the earthquake can be di-

ISBN 978-3-8007-4636-1 / ISSN 2197-4403

rectly computed from the differential interferometric phase.

5 Results

In this section, intermediate results from the processing of both topographic and differential image pairs are presented, respectively the flattened and unwrapped interferometric phases.

Flattened phase of the interferometric image pair is presented in **Figure 5**. The expectation that topographic component is dominant in this image pair is validated by the fact that altitude variation are clearly visible in the flattened interferometric phase.

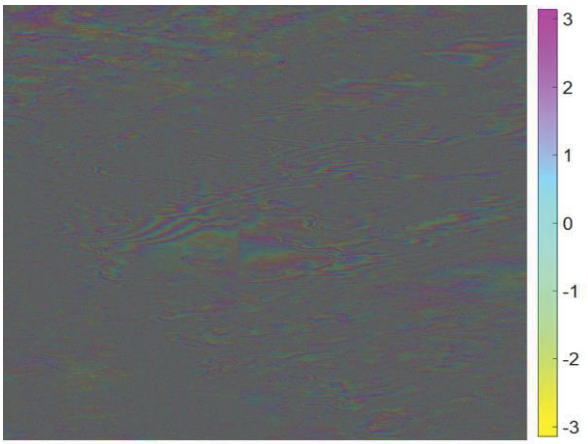

Figure 5: Flattened interferometric phase of the topographic pair

Landform is also prevailing in the unwrapped topographic phase, as it can be noticed in **Figure 6**. No major discontinuities are induced by the unwrapping process, the performant adaptive filtering and unwrapping algorithms making possible the preservation of topographic information.

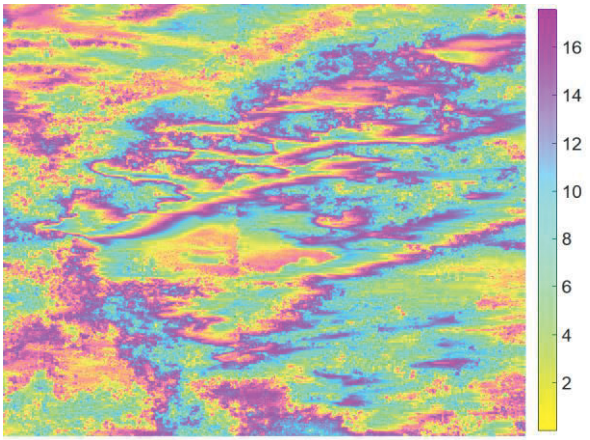

Figure 6: Unwrapped phase of the topographic image

Altitude changes are predominant only in restricted areas from the flattened interferogram of the differential pair – **Figure 7**. It is also observable that, as expected, coherence of this pair is lower than the one of interferometric pair, an assumption also confirmed by comparison of the spectral coherence maps generated by the adaptive filtering.

Figure 7: Flattened interferometric phase of the differential pair

In the unwrapped phase of the differential pair, presented in **Figure 8**, the altitude changes are overlaid with the displacements caused by the earthquake. As a consequence, the topographic texture of the scene is no longer evident. Also, because the coherence of differential pair is lower, the interferometric phase has a noisier aspect.

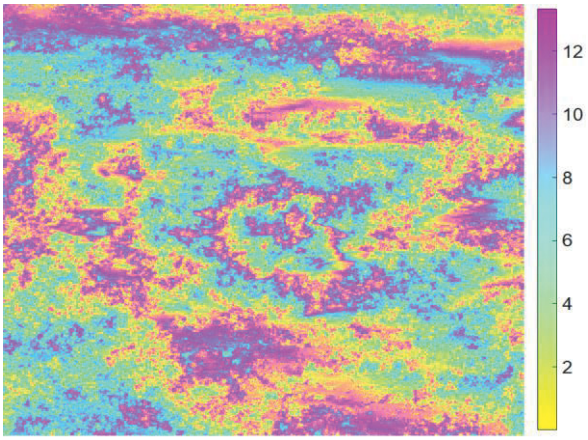

Figure 8: Unwrapped phase of the differential image pair

The displacements are obtained by appropriate combination of the two unwrapped interferograms, followed by conversion of the differential interferometric phase to deformation values. Spatial variation of the displacements estimated in vertical direction is shown in **Figure 9**.

ISBN 978-3-8007-4636-1 / ISSN 2197-4403

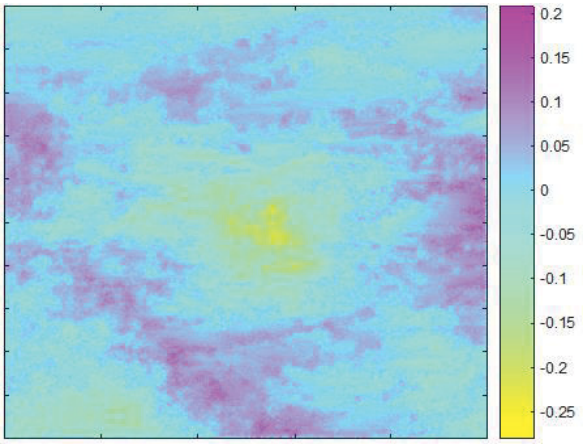

Figure 9: Estimated vertical displacements (cm) caused by Italy's 30.10.2016 earthquake, Perugia region

The range of estimated displacements in vertical direction varies between -28.05 and 20.85 cm.

6 Conclusions

The specific contribution presented in this paper consists in employment of 3-pass differential interferometry for estimation of October 2016 central Italy earthquake's displacements. Main differences compared to 2-pass D-InSAR, employed in most works from interferometry domain literature, and 3-pass approach adopted in this paper were presented.

Selection of suitable image pairs for topographic and displacements components estimation is eased by the availability, high coverage and reduced revisit time of the Sentinel-1 images acquired in TOPS mode. However, accurate co-registration of dataset's proved vital.

The estimation of the displacements caused by the mentioned earthquake was also conducted by the research group of CNR-IREA [13], using 2-pass D-InSAR. The validation of the results presented in this article was implemented by comparison with the displacements maps generated by IREA researchers: The vertical displacements presented in [13] belong to -30:30 cm domain, so the values estimated in this article are comparable. The spatial distribution of the displacements are also similar in both maps. In conclusion, 3-pass D-InSAR also proved to be a valid method for estimation of natural disasters effects.

Acknowledgements

Authors wish to thank Antonio Pepe and Gianfranco Fornaro from CNR-IREA, Italy for their suggestions regarding the paper framing. This work has been conducted within the frame of research project *SPERO – Space technologies used in the management of disasters and major crises, manifested at local, national and regional levels*, funded from the Minister of Research and Innovation, UEFISCDI, project reference: PN-III-P2-2.1-SOL-2016-03-0046

References

[1] Curlander, John C., and Robert N. McDonough. *Synthetic aperture radar*. New York, NY, USA: John Wiley & Sons, 1991.

[2] Bamler, R. "Principles of synthetic aperture radar." *Surveys in Geophysics* 21.2 (2000): 147-157.

[3] Rosen, P. A., Hensley, S., Joughin, I. R., Li, F. K., Madsen, S. N., Rodriguez, E., & Goldstein, R. M. "Synthetic aperture radar interferometry". *Proceedings of the IEEE*, *88*(3), (2000): 333-382

[4] Bamler, R and Hartl, P. "Synthetic aperture radar interferometry" *Inverse problems* 14.4, (1998)

[5] Strozzi, T., Wegmuller, U., Tosi, L., Bitelli, G., & Spreckels, V. "Land subsidence monitoring with differential SAR interferometry". *Photogrammetric engineering and remote sensing*, *67*(11), (2001): 1261-1270

[6] Lanari, R., et al. "Sentinel-1 results: SBAS-DInSAR processing chain developments and land subsidence analysis." *Geoscience and Remote Sensing Symposium (IGARSS), IEEE International*. IEEE, (2015)

[7] Strozzi, T. "Validation of the X-SAR SRTM DEM for ERS and JERS SAR geocoding and 2-pass differential interferometry in alpine regions." *Geoscience and Remote Sensing Symposium, IEEE International*. (2003).

[8] *** - Gamma Interferometric SAR Processor, ISP User's Guide, (2014)

[9] *** - Gamma Interferometric SAR Processor, DIFF&GEO User's Guide, (2014)

[10] Goldstein, R. M., & Werner, C. L. "Radar interferogram filtering for geophysical applications". *Geophysical research letters*, *25*(21), (1998): 4035-4038.

[11] Ojha, C, M. Manunta, R. Lanari and A. Pepe, "The Constrained-Network Propagation (C-NetP) Technique to Improve SBAS-DInSAR Deformation Time Series Retrieval," in IEEE JSTARS, vol. 8, no. 10, pp. 4910-4921, Oct. 2015

[12] Chew, L.P. "Constrained Delaunay triangulations," in Algorithmica, vol. 4, Springer. Verlag. New York 1989, pp. 97–108.

[13] http://www.esa.int/Our_Activities/Observing_the_Earth/Copernicus/Sentinel1/Sentinel_satellites_reveal_east_west_shift_in_Italian_quake